Antihelical edge magnons in patterned antiferromagnetic thin films

Yun-Mei Li*

Department of Physics, School of Physical Science and Technology, Xiamen University, Xiamen 361005, China

(Received 16 March 2023; revised 2 June 2023; accepted 26 June 2023; published 13 July 2023)

Helical edge states in topological insulators generate a counterpropagating spin current on the two parallel edges. We here propose antihelical edge states of magnons in patterned antiferromagnetic thin films, which host a copropagating spin current on the two parallel edges, where the two magnon modes with opposite chirality act like the spin. The embedded heavy metal dot array in the thin film induces interfacial Dzyaloshinskii-Moriya interactions (iDMIs), drives the magnon bands into nontrivial topological phases, characterized by spin Chern number. The resulting helical edge modes lead to spin current with the direction dependent on the sign of the iDMI parameter. In a strip geometry, we combine two subsystems with two embedded metal dot arrays, which give opposite iDMI parameters. Antihelical edge states emerge, compensated by the counterpropagating bulk-confined states. Helical and antihelical edge states are verified by the micromagnetic simulations. We consider these results promising and inspiring for further developments of magnon spintronic devices based on antiferromagnets.

DOI: 10.1103/PhysRevResearch.5.033026

I. INTRODUCTION

Chiral or helical edge states are a hallmark feature of two-dimensional topological insulators [1,2]. Chiral edge states emerge in quantum Hall or Chern insulators with time-reversal symmetry breaking and propagate along the edges either clockwise or counterclockwise. As a consequence, a typical strip geometry supports opposite propagating edge states along the two parallel edges. Helical edge states can be treated as two copies of chiral edge states, protected by the time-reversal symmetry, holding great potential applications in spintronics. The edge states for opposite spin hold opposite chirality, compensating the charge current with the net spin current flowing in the opposite direction along parallel edges in the narrow strip geometry considered.

Recent theory predicted the so-called antichiral edge states [3], which copropagate in the same direction at opposite edges, compensated by counterpropagating bulk modes, distinct from the chiral edge states. The original hypothesis was based on the modified Haldane model in electronic systems [3], which is considerably difficult for experimental implementation. Nevertheless, many theoretical and experimental works followed, reporting the possible realization of this mechanism in a large variety of systems, including electrons in graphene [4,5], the exciton polariton [6], magnon [7], photon [8,9], and classical electric circuit systems [10]. The experimental works in photonic [9] and electric circuit [10] systems observed the copropagating behavior of antichiral edge states based on the modified Haldane model. All these reports suggested the use of the systems with broken time-reversal symmetry. A natural question arises: Is it possible to realize "antihelical" edge states in the time-reversal symmetric systems where the spin current on the parallel edges propagates in the same direction? Only a few theoretical and experimental results were published in this direction to date [11].

In recent yeas, antiferromagnets have attracted significant attention in spintronics due to the ultrafast spin dynamics and lack of stray fields [12,13]. Importantly, antiferromagnets support both left-handed and right-handed polarized magnon modes, related by the pseudotime reversal symmetry [14], analogous to the electron spin. This coexistence of both polarizations gives rise to many novel spin-related physical phenomena, such as the magnon spin Nernst effect [15,16], the Stern-Gerlach effect [17], and the Hanle effect [18]. Manipulating the polarization may facilitate the chirality-based computing [19,20] and logic devices [21]. Therefore, the exploration on topologically protected helical or even antihelical edge state could be greatly helpful in the field of magnon spintronics based on antiferromagnets [22].

In this paper, we report theoretical results concerning the possible realization of antihelical edge states of magnons in the patterned antiferromagnetic thin film in which the spin currents at parallel edges flow in the same direction, compensated by the counterpropagating bulk-confined spin currents, as illustrated in Fig. 1(a). Here the degenerate two magnon modes with opposite chirality are treated as the spin degree of freedom, an approach already taken in the previous works mentioned above. The heavy metal dot array is embedded into the thin film to fold the free dispersion of magnons into bands. Moreover, the inversion symmetry breaking at the interfaces between metal dots and the thin film will generate interfacial

*yunmeili@xmu.edu.cn

Published by the American Physical Society under the terms of the Creative Commons Attribution 4.0 International license. Further distribution of this work must maintain attribution to the author(s) and the published article's title, journal citation, and DOI.

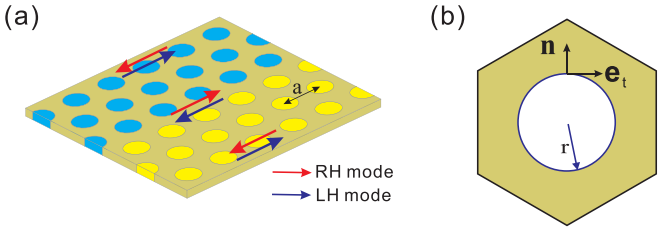

FIG. 1. (a) The illustration of antihelical edge spin waves in a patterned antiferromagnetic thin film. The heavy metal dot array is arranged in a triangular lattice configuration. We consider the metal dot array being formed of two different metals, resulting in antihelical edge states. The distance between the metal dot center is a. (b) Top view of the unit cell for the antiferromagnetic thin film when only one type of metal dot is embedded. The vectors $\mathbf{n}$ and $\mathbf{e}_t$ are the normal and in-plane tangential vectors of the interfaces, respectively. The radius of the metal dot is r.

Dzyaloshinskii-Moriya interactions (iDMIs), which modify the exchange boundary condition and induce a nontrivial topological phase for the magnon bands, characterized by the spin Chern number. As a result, helical edge magnons arise in a finite-width strip geometry. The left-handed and right-handed edge magnons flow in opposite directions at the same edge, leading to a pure spin current, which is confirmed with micromagnetic simulations. The direction of the edge spin current is determined by the sign of iDMI parameter D. In a finite-width ribbon geometry, we combine two subsystems embedded with different metal dot arrays, which are assumed to induce iDMIs with opposite sign of D, as shown in Fig. 1(a). Importantly, the spin currents are flowing in the same direction, while those at the domain boundary go in the opposite direction. The emergence of the antihelical edge states is also confirmed by the micromagnetic simulations.

This paper is organized as follows. In Sec. II, we derive the eigenvalue problem for the magnons in the patterned antiferromagnetic thin film in the presence of metal dot array and the iDMIs. In Sec. III, we discuss the band topological properties due to the iDMIs, the topological phase transitions and the construction of strip geometry supporting antihelical edge states. Micromagnetic simulations were performed to confirm and verify the analytical results. In Sec. IV, we summarize our results. In Sec. V, we describe calculation methods and list the main parameters used in the numerical calculations.

II. PATTERNED ANTIFERROMAGNETIC THIN FILM

We consider thin antiferromagnetic film with a periodic array of embedded heavy metal dots, which form a triangular lattice. Two magnetic domains can be constructed by using two different metals in the top and bottom halves of the sample. This approach permits achieving antihelical edge states [Fig. 1(a)]. An infinite system with only one type of embedded metal dot array is a two-dimensional artificial magnonic crystal. The corresponding unit cell is shown in Fig. 1(b). The strip geometry with one or two embedded metal dot arrays is a one-dimensional artificial magnonic crystal. The magnetization dynamics in antiferromagnets can be described by two coupled Landau-Lifshitz-Gilbert (LLG) equations for each sublattice

$$\dot{\mathbf{m}}_i = -\gamma \mathbf{m}_i \times \mathbf{h}_i + \alpha \mathbf{m}_i \times \dot{\mathbf{m}}_i, \tag{1}$$

where $i = 1, 2$ denote the two sublattices. γ is the gyromagnetic ratio, α is the Gilbert damping constant. Here $\gamma \mathbf{h}_i = K_z m_i^z \mathbf{z} + A\nabla^2 \mathbf{m}_i - J_{\rm ex}\mathbf{m}_{\bar{i}}$ (with $\bar{1} = 2$ and $\bar{2} = 1$) is the effective magnetic field acting locally on sublattice $\mathbf{m}_i$, where K_z is the easy-axis anisotropy along the $\mathbf{z}$ direction A and $J_{\rm ex}$ characterize the Heisenberg exchange coupling constant of the intrasublattice and intersublattice, respectively. The equilibrium magnetization is in collinear order for the two sublattices and parallel to the z-direction. To get the magnon dispersions, we can divide the magnetization and effective magnetic fields on each sublattice into the static and dynamical ones. Let $\mathbf{m}_i = \mathbf{m}_i^0 + \delta\mathbf{m}_i$ and $\mathbf{h}_i = \mathbf{h}_{i,0} + \delta\mathbf{h}_i$ with $\mathbf{m}_i^0$ the equilibrium magnetization and $|\delta\mathbf{m}_i| \ll \mathbf{m}_i^0$. $\mathbf{h}_{i,0}$ is the z-component of the effective magnetic field. By neglecting the damping, we have $\partial\delta\mathbf{m}_i/\partial t = -\gamma(\mathbf{m}_i^0 \times \delta\mathbf{h}_i + \delta\mathbf{m}_i \times \mathbf{h}_{i,0})$. To solve the dispersion in the artificial crystals, we employ the ansatz $\delta\mathbf{m}_i = \delta\mathbf{m}_i^{\mathbf{k}}(\mathbf{r})e^{i(\mathbf{k}\cdot\mathbf{r}-\omega t)}$, and after a transformation, we can get the eigenvalue equations, given by

$$\omega\psi_{\pm,\mathbf{k}} = \mp\sigma_z \hat{H}_{\mathbf{k}}\psi_{\pm,\mathbf{k}}, \tag{2}$$

where $\psi_{\pm,\mathbf{k}} = (\delta m_{1,\pm}^{\mathbf{k}}, \delta m_{2,\pm}^{\mathbf{k}})^T$, $\delta m_{i,\pm}^{\mathbf{k}} = \delta m_{i,x}^{\mathbf{k}} \pm i\delta m_{i,y}^{\mathbf{k}}$, $\hat{H}_{\mathbf{k}} = [K_z + J_{ex} + (\nabla + i\mathbf{k})^2]\sigma_0 + J_{\rm ex}\sigma_x$. σ_0 is 2×2 identity matrix, $\sigma_{x,y,z}$ are the Pauli matrices. The solution for $\psi_{+,\mathbf{k}}$ denotes left-handed modes while $\psi_{-,\mathbf{k}}$ is the solution for right-handed modes. As discussed in our recent work [14], the two polarized modes are totally decoupled but related by a pseudotime reversal symmetry. Besides the above classical treatment to get the spin wave solution, we can also make the Holstein-Primakoff (HP) transformation for the magnetization [23,24] and neglect the magnon-magnon interaction to get a quantum description $\delta m_{1,+}^{\mathbf{k}} \propto \sqrt{\frac{2}{M_s}}a_{\mathbf{k}}$, $\delta m_{1,-}^{\mathbf{k}} \propto \sqrt{\frac{2}{M_s}}a_{\mathbf{k}}^\dagger$, $\delta m_{2,+}^{\mathbf{k}} \propto \sqrt{\frac{2}{M_s}}b_{\mathbf{k}}^\dagger$, $\delta m_{2,-}^{\mathbf{k}} \propto \sqrt{\frac{2}{M_s}}b_{\mathbf{k}}$. Then the above eigenvalue equation in Eq. (2) becomes a fully quantum version, corresponding to the Heisenberg equation of motion for HP boson operators with monochromatic solution. In our work, considering the large lattice constant of the artificial magnonic crystal and the nontrivial boundary condition due to the metal dots discussed below, we still apply the convenient classical approach to discuss the spin-wave dispersion and the topological properties.

We turn to the role of the embedded heavy metal dots. The first effect is to fold the free dispersion into magnon bands due to the scattering by the periodic interfaces from the metals. More importantly, as discussed in many theoretical [25–30] and verified in experimental works [31–35], the heavy metals (such as Pt, W, Au, Re, Ir, etc.) with strong spin-orbit coupling can generate chiral interfacial Dzyaloshinskii-Moriya interactions (iDMI) due to the inversion symmetry breaking at the magnets/heavy metal interfaces. In our system, the iDMI $\mathbf{h}_{\rm DM}$ is given by $\gamma\mathbf{h}_{\rm DM} = D\mathbf{z} \times (\mathbf{e}_t \cdot \nabla)\mathbf{m}_i$ by comparing our curvilinear surfaces to the previous plane surface [26,35]. $\mathbf{e}_t = \mathbf{n} \times \mathbf{z}$ is the in-plane tangential vector of the interface and $\mathbf{n}$ the normal vector of the interface, both depicted in Fig. 1(b). D may be either positive or negative, depending on the metal materials [27,28]. Without loss of generality, we

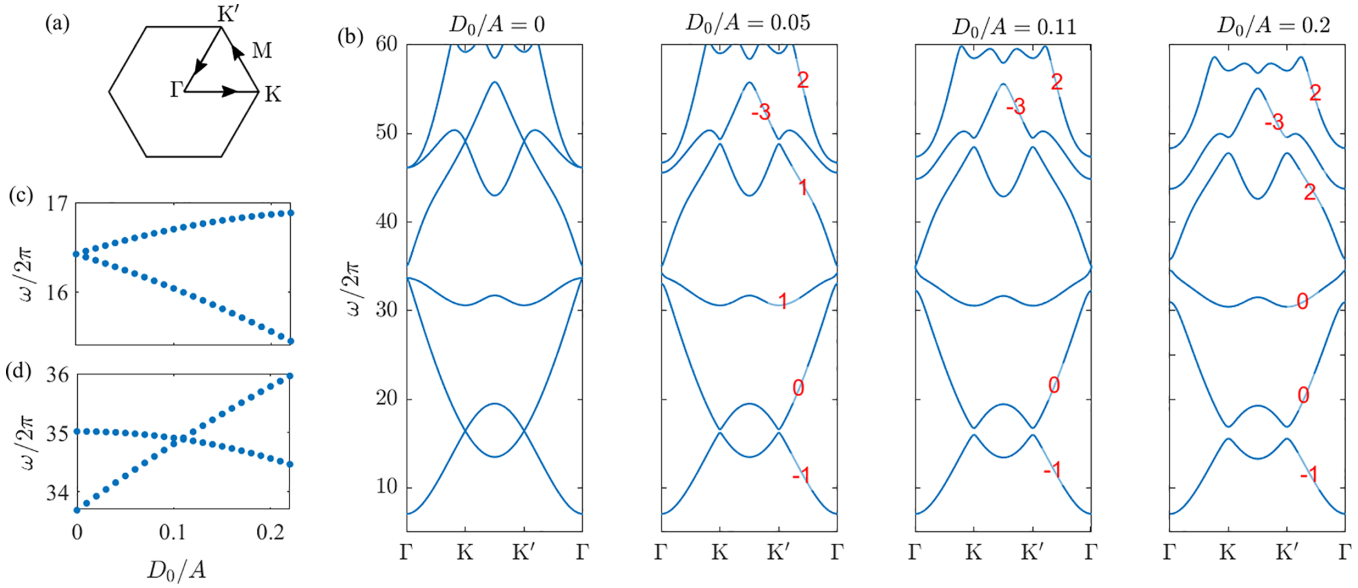

FIG. 2. (a) The Brillouin zone and the path illustration for plotting the bands. (b) The band diagrams for the right-handed magnon modes calculated for $D_0 = 0$, $D_0 = 0.05A$, $D_0 = 0.11A$, and $D_0/A = 0.2A$, respectively. The left-handed modes are degenerate to the right-handed ones. The Chern numbers for each band are indicated in red. The Chern numbers for the left-handed modes are opposite. (c) The dependence of the eigenfrequency for the first and second bands at the K (K') point with respect to D_0. (d) The dependence of the eigenfrequency for the third and fourth bands at the Γ point with respect to D_0.

assume D is uniform at the curvilinear surfaces. The iDMI will give an interfacial torque [29] and change the exchange boundary condition into the formalism below:

$$\mathbf{n} \cdot \nabla \mathbf{m}_i + \frac{Dd}{A} \mathbf{z} \times (\mathbf{e}_t \cdot \nabla)\mathbf{m}_i = 0, \tag{3}$$

with d the thickness of interface atomic layer and $D_0 = Dd$ is a constant, only depending on the materials. This constant D_0 value accounts for the experimentally observed approximately inverse thickness dependence of spin-wave frequency shift in ferromagnets/heavy metal heterostructures [33,34].

By solving the eigenvalue equation in Eq. (2) with the nontrivial boundary condition in Eq. (3), we can obtain the magnon dispersions in the $\mathbf{k}$-space. The strip geometry illustrated in Fig. 1(a) can also be calculated. The results are shown in the subsequent section.

III. RESULTS AND DISCUSSIONS

A. Band topological phase transitions

Before addressing the antihelical edge states, we first discuss the topological properties of magnons in the thin AFM film containing an embedded array composed of a single type of heavy metal dots. The corresponding Brillouin zone (BZ) is shown in Fig. 2(a). We present the band dispersions at four different D_0 values for the right-handed modes in Fig. 2(b). The left-handed bands are degenerate to the right-handed ones. When $D = 0$, all the bands are topological trivial. The first (fourth) and second (fifth) bands are degenerate at the K and K' points, which gives multiple Dirac points in the spectrum. The second (fifth) and third (sixth) bands intersect at the Γ point.

A finite D lifts all the above the band degeneracies and open band gap at Γ, K, and K' points. As the right-handed and left-handed modes are totally decoupled, we can use the Chern number to characterize the topological properties for the bands of each polarized mode. The Berry connection of the nth band is given by $\mathbf{A}^{\mathbf{k}}_{n,\pm} = \mp i \int_{uc} \psi^{n,\dagger}_{\pm,\mathbf{k}} \sigma_z \nabla_{\mathbf{k}} \psi^{n}_{\pm,\mathbf{k}} d\mathbf{r}$ and Berry curvature $\mathbf{B}^{\mathbf{k}}_{n,\pm} = \nabla_{\mathbf{k}} \times \mathbf{A}^{\mathbf{k}}_{n,\pm}$. The Chern number $C_{n,\pm} = \frac{1}{2\pi} \int_{\mathrm{BZ}} B^{\mathbf{k}}_{n,z,\pm} d^2\mathbf{k}$. The integral for the Berry connection is done over the unit cell. The Chern number for the corresponding right-handed magnon bands are shown in Fig. 2(b) by the number on the bands. We find the Chern numbers for the left-handed magnon bands are opposite to the right-handed ones for each degenerate band. Therefore, we can use the spin Chern number to characterize the topological properties of the total system, $C_{n,s} = (C_{n,-} - C_{n,+})/2$. We can also define the nth gap spin Chern number $\bar{C}_{n,s}$ associated with the gap above the nth band as

$$\bar{C}_{n,s} = \sum_{n'=1}^{n} C_{n',s}. \tag{4}$$

The number $\bar{C}_{n,s}$ determines the number of helical edge states in the nth gap according to the bulk-boundary correspondence. When D reverses sign, the Chern number for each mode will reverse the sign accordingly. The spin Chern number will also reverse sign. Therefore, the spin current due to the helical edge states are expected to change the flow direction. As the sign of D is determined by the heavy metal materials, we can design our system by choosing the heavy metal as desired. Based on this feature, we can construct the antihelical edge magnons by structural design.

For the first gap, a larger D will give a larger band gap at the K and K' points, as shown in Fig. 2(c). At any value of D, the spin Chern number of the first gap is always -1. Interestingly, increasing D will drive a topological phase transition for the third and fourth bands. We find when $D_0 = D_0^c \simeq 0.11A$, the band gap between the third and fourth bands at the Γ point will be closed. A larger D_0 will reopen the gap, as shown

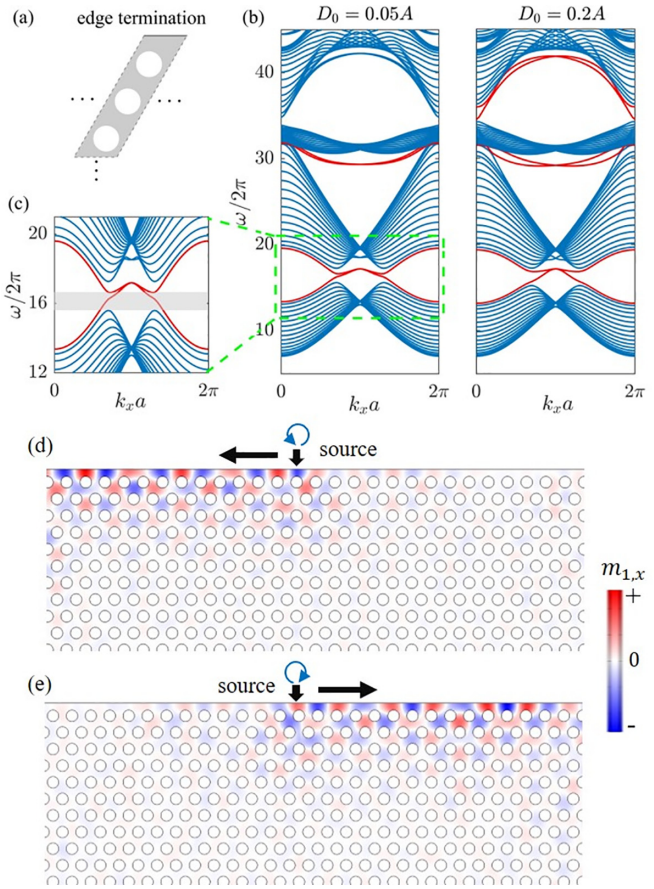

FIG. 3. (a) The illustration of the edge termination on the upper edge for the finite width ribbon with a single type of heavy metal dots embedded. (b) Band dispersion diagrams for the right-handed magnons in the ribbon calculated for $D_0 = 0.05A$ and $D_0 = 0.2A$, respectively. The left-handed magnon bands are degenerate to the right-handed ones. The edge states are displayed with red curves. The width of the ribbon is 716 nm. (c) Zoomed-in part of the band diagram calculated for $D_0 = 0.05A$ from the green dashed box shown in (b). (d) Snapshot of right-handed spin wave propagation at frequency $\omega/2\pi = 16.2$ GHz. (e) Snapshot of left-handed spin wave propagation at frequency $\omega/2\pi = 16.2$ GHz. (d),(e) $D_0 = 0.2A$. Black arrows labeled "source" mark the position of the microwave antenna.

in Figs. 2(b) and 2(d). The spin Chern number for the third band $C_{3,s}$ will change from 1 to 0, while for the fourth band, $C_{4,s}$ changes from 1 to 2. The total (spin) Chern number of the two bands remain unchanged. But this topological phase transition will change the third gap spin Chern number $\bar{C}_{3,s}$ from 0 to -1. This indicates that the third gap will experience a topologically trivial to nontrivial phase transition. From Fig. 2(b) we can see only the first and third band gap are full gaps.

B. Helical edge magnons

The nonvanishing nth gap spin Chern number is expected to give rise to helical edge states covering the band gap. To verify this prediction, we calculate the band dispersion in a strip geometry with a finite width along the y direction and infinite along the x direction. The strip geometry with only upper edge termination is presented in Fig. 3(a). The band diagrams for the ribbon-like system, calculated for the right-handed modes, are shown in Fig. 3(b) with $D_0 = 0.05A$ (left) and $D_0 = 0.2A$ (right), respectively. The bands for left-handed modes are degenerate to the right-handed ones. For $D_0 = 0.05A$, the edge states still can be see in the first and second band gaps. The spin Chern number of the third gap is 0, indicating a trivial gap without supporting edge states. Edge states are also expected to exist in higher bands. But due to the absence of full gaps, they are not distinguishable from the bulk states, and thus not illustrated. For $D_0 = 0.2A$, the edge states in the first and second gaps remain in place. Additional edge states emerge in the third band gap due to the topological phase transition for $D_0 > D_0^c$ compared to $D_0 < D_0^c$.

The zoomed-in image of the band diagram calculated for $D_0 = 0.05A$ in the vicinity of the first band gap [Fig. 3(c)]reveals that the edge states with the frequency located in the shaded region correspond to purely chiral features. These edge states thus propagate unidirectionally. We can also see this feature for the states in the first and third gaps for $D_0 = 0.2A$. The excitation of the states with other frequencies in the first gap and the states in the second gap will do not show unidirectional flow. In the subsequent simulations, we mainly focus on the states in the first band gap. Due to the helical nature of the edge states, spin current flows principally at the edges of the ribbon. To verify the presence of topologically protected edge magnons, we perform micromagnetic simulations by selectively exciting spin waves of left-handed and right-handed polarizations. The details of micromagnetic simulations is presented in Sec. V. The results are shown in Figs. 3(d) and 3(e). We apply a right-handed microwave source with the frequency corresponding to the first band gap. The excited right-handed spin waves propagate to the left [Fig. 3(d)], consistent with the in-pane magnetization distributions obtained from band calculation. When we changed the microwave source to the left-handed one, the excited spin waves propagates to the right [Fig. 3(e)]. When the excitation microwave source is linearly polarized, both magnon modes will be excited. A higher frequency oscillation corresponding to the third band gap will also feature the same behavior. When the excitation source is placed in the opposite parallel edge, the moving direction of each mode will be opposite. The obtained dynamics of excited spin waves confirm the helical nature of the edge states. Similarly, in the case of electron systems, it will cause magnon spin currents at the edges, propagating in the opposite direction. These states are topologically protected and are thus robust against the disorders from the nanofabrication process. Similar results were already reported in a previous work [36].

The sign of the spin Chern number is locked to the sign of iDMI parameter D, which is dependent on the heavy metal materials. When we embed different heavy metal dot arrays to induce an opposite D, both polarized edge states will change the direction of their propagation. Spin currents will also reverse their directions. This feature in our system is the key point for the construction of antihelical edge states.

C. Antihelical edge magnons

Based on the locking behavior between spin Chern number and D, we now construct the antihelical edge magnons in our

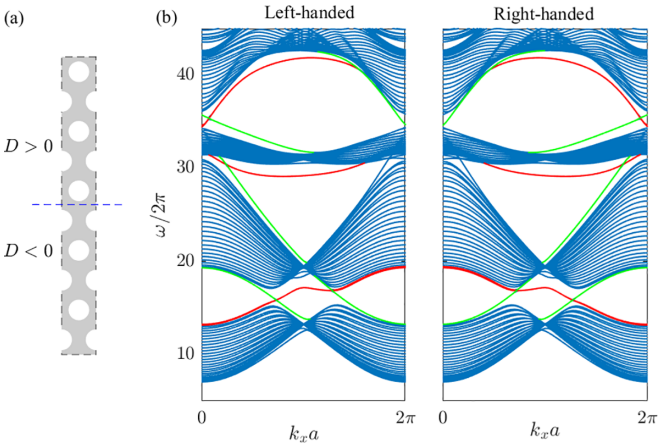

FIG. 4. (a) Ribbon geometry required for the formation of antihelical edge states. Blue dashed line marks the boundary between two arrays of embedded heavy metal dots. These metals should be different for producing the opposite signs of D in the iDMI. (b) The band dispersion for the left-handed and right-handed modes for the configuration shown in (a). The width of the of the ribbons is 1236 nm. The edge states are marked with red curves. The edge states confined at the interface between two types of metal dot arrays are displayed in green. Doubly degenerate edge states are localized at the upper and lower edges, respectively. The absolute value of D_0 used in our calculation is $0.2A$.

system that the edge spin currents at the parallel edges will flow in the same direction. As the the sign of D is determined by the heavy metal materials, we create the domain boundary at the middle of the strip [Fig. 1(a)]by using two different types of metal dots at the either side from the interface. The two metal materials are assumed to induce iDMI with opposite D, as illustrated in Fig. 4(a). For simplicity, we assume the absolute value of D is the same. The different absolute value of D will lead to quantitatively similar physical picture.

We plot the bands for both polarized modes in Fig. 4(b) at $|D_0| = 0.2A$. The edge states are marked in red. The green color is used for the modes localized along the interface between the two domains with different embedded heavy metal dot arrays. These edge and interfacial states are still topologically protected. The edge modes are doubly degenerate for both spin polarizations at the upper and lower edges. For each polarized edge state covering the first and third gaps, the two degenerate states propagate in the same direction, while the states at the interface propagate in opposite directions. The left-handed polarized bands can be mirrored to the right-handed ones with respect to $k_x a = \pi$ (time-reversal invariant point) and vice versa. On each edge and on the interface, two polarized modes flow in contrast to each other.

The antihelical feature of the edge magnons can also be revealed in the micromagnetic simulations. The results are shown in Figs. 5(a) and 5(b). The excited left-handed spin waves on the parallel edges flow towards the right while the interfacial ones flow to the left. On the contrary, the excited right-handed edge spin waves propagate to the left and the interfacial ones propagate to the right. These behaviors demonstrate the successful construction of antihelical edge magnons. In a cell with a finite width along the x direction, a linearly polarized microwave source will excite both polarized spin waves, as shown in Fig. 5(c). When the spin waves meet the left and right vertical edges, they will be totally transmitted without backscattering due to the topological protection. But they cannot propagate into the bottom part of the system because of the antihelicity: polarized magnons moving along vertical edges can travel only along the interface [Fig. 5(c)]. Upon reaching the opposite vertical edge, they will split into two flows, one of which can be partially transmitted to the bottom part of the system [Fig. 5(c), inset]. Therefore, all magnons traveling along the edges can move between the upper and lower parts of the system only after propagating along the interface separating them.

D. Discussions

Above all, we discussed the band topology due to the iDMIs, in addition to the helical and the antihelical edge magnons in the patterned antiferromagnetic thin film. In our calculations, the thickness of the film is 4 nm. If another thickness value is chosen, the same band dispersion will be

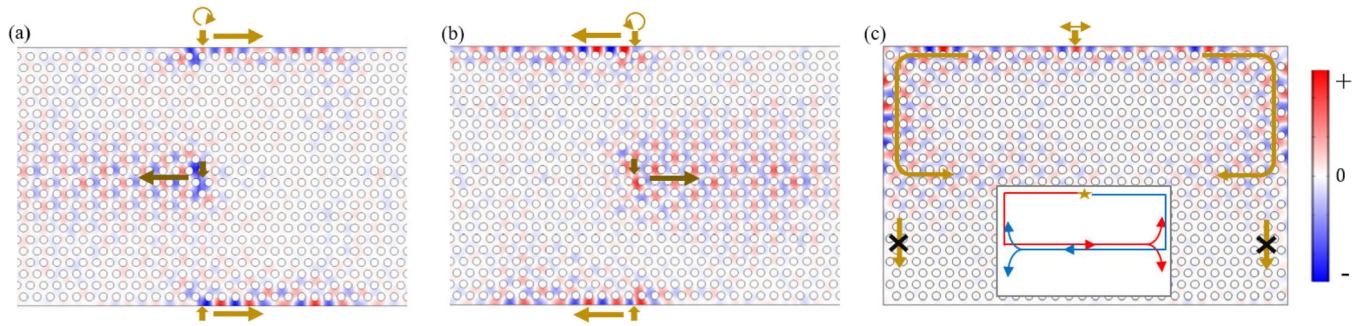

FIG. 5. Propagation of spin waves excited by microwave antennas, which are marked with short vertical arrows in the figure. The excitation frequency is $\omega/2\pi = 16.2$ GHz. (a) Left-handed spin waves move to the right along the edges while the confined modes at the interface move to the left. (b) Right-handed spin waves move to the left along the edges while the confined modes at the interface move to the right. The color scheme for panels (a) and (b) corresponds to the $m_{1,x}$. (c) Spin-wave propagation from a linearly polarized microwave source, which excites both left- and right-handed modes. The propagation paths are shown in the inset with red (blue) denoting the right-handed (left-handed) modes. The color scheme for panel (c) shows $n_y = m_{1,y} - m_{2,y}$. The illustrated results are obtained with micromagnetic calculations over the 1500 nm× 975 nm grid.

observed if we focus only on bulk modes with $k_z = 0$. The modes with higher frequency at nonvanishing k_z for any film thickness are also expected to give the same physics as any k_z mode shares the same symmetry in the xy plane. We adopt the triangular symmetry for the embedded array of heavy metal dots. For the other array configuration (for example, a square lattice), a similar magnon dynamics is expected.

We here adopted a medium lattice constant ($a = 50$ nm) for the calculations. A larger lattice constant is not likely to alter the topological properties of the magnon bands but will give a smaller band gap, making it harder to observe the edge and interfacial states. For example, when the lattice constant and radius of the metal dot are both doubled with $D_0 = 0.2A$, the value of the first band gap at K will decrease from $\Delta\omega/2\pi =$ 1.3 GHz to 0.45 GHz. In realistic experiments, a proper lattice constant should be chosen considering both the experimental detection and difficulties from nanofabrication. The helical, antihelical, and interfacial states can be probed in the spin pumping process as opposite magnon chirality could generate opposite spin polarization, discussed in a recent experimental work [37]. They can also be detected by the polarization selective spectroscopy [38]. In addition, our configuration in a ferromagnetic thin film will lead to the antichiral edge states as there is only one magnon polarization in ferromagnets.

IV. SUMMARY

We propose a theoretical framework for realizing antihelical edge magnons in antiferromagnetic thin film with an embedded array of heavy metal dots. The iDMIs induce helical edge states with the direction of spin current dependent on the sign of the iDMI parameter. The system can be efficiently split into two working areas by embedding two different types of metal dots. Such a subdivision will favor the opposite direction of spin current flows at the long edges of the system and at the interface. The proposed system is experimentally feasible. The new methods for controlling magnon spin currents in antiferromagnets suggested here can be promising for the development and improvement of magnon spintronic devices based on antiferromagnetic materials.

V. METHODS

The band calculation and micromagnetic simulations are performed by using the software COMSOL MULTIPHYSICS, where the eigenvalue problem and the Landau-Lifshitz-Gilbert (LLG) equation are transformed into the coefficient forms by using the mathematical module. The nearest distance between the metal dot center (lattice constant) is $a = 50$ nm. The radius of the metal dot is $r = 15$ nm. The parameters in the coupled LLG equation are as follows [39]: $K_z = 8.55$ GHz, $A = 7.25 \times 10^{-6}$ Hz $\cdot$ m^2, $J_{ex} = 1.105 \times 10^{11}$ Hz. The saturation magnetization $M_s = 1.94 \times 10^5$ A/m, the gyromagnetic ratio $\gamma = 2.21 \times 10^5$ Hz $\cdot$ m/A. The values of D_0 in the unit of A are given in the main text according to our need for the discussions. The micromagnetic simulation is based on Eq. (1). The damping constant is adopted as $\alpha = 2 \times 10^{-4}$ to get a long decay length. We did not take the dipolar fields into calculation due to the antiferromagnet environment. The temperature for the calculation is choose to be $T = 0$ K and no stochastic noise is considered.

We can selectively excite either one or both of the polarized modes simultaneously by setting the microwave fields. The effective field of the radio wave is given by $\mathbf{h}_{rf}(t) = h_0[\cos(\omega t)\mathbf{e}_x \pm \sin(\omega t)\mathbf{e}_y]$, where $+$ denotes the right-handed source and $-$ denotes the left-handed source. Only one component above along the x or y direction give a linearly polarized source. In our micromagnetic simulation $h_0 = 2 \times 10^9$ Hz, $\omega = 2\pi \times 16.2$ GHz.

ACKNOWLEDGMENTS

Y.-M.L. thanks Prof. Kai Chang and Dr. Yongwei Huang for their helpful discussions. This work is supported by Grant No. 2022YFA1204700 from the MOST of China and the startup funding from Xiamen University.

[1] M. Z. Hasan and C. L. Kane, Colloquium: Topological insulators, Rev. Mod. Phys. **82**, 3045 (2010).
[2] X.-L. Qi and S.-C. Zhang, Topological insulators and superconductors, Rev. Mod. Phys. **83**, 1057 (2011).
[3] E. Colomés and M. Franz, Antichiral Edge States in a Modified Haldane Nanoribbon, Phys. Rev. Lett. **120**, 086603 (2018).
[4] M. M. Denner, J. L. Lado, and O. Zilberberg, Antichiral states in twisted graphene multilayers, Phys. Rev. Res. **2**, 043190 (2020).
[5] X. Cheng, J. Chen, L. Zhang, L. Xiao, and S. Jia, Antichiral edge states and hinge states based on the Haldane model, Phys. Rev. B **104**, L081401 (2021).
[6] S. Mandal, R. Ge, and T. C. H. Liew, Antichiral edge states in an exciton polariton strip, Phys. Rev. B **99**, 115423 (2019).
[7] D. Bhowmick and P. Sengupta, Antichiral edge states in Heisenberg ferromagnet on a honeycomb lattice, Phys. Rev. B **101**, 195133 (2020).
[8] J. Chen, W. Liang, and Z.-Y. Li, Antichiral one-way edge states in a gyromagnetic photonic crystal, Phys. Rev. B **101**, 214102 (2020).
[9] P. Zhou, G.-G. Liu, Y. Yang, Y.-H. Hu, S. Ma, H. Xue, Q. Wang, L. Deng, and B. Zhang, Observation of Photonic Antichiral Edge States, Phys. Rev. Lett. **125**, 263603 (2020).
[10] Y. Yang, D. Zhu, Z. Hang, and Y. Chong, Observation of antichiral edge states in a circuit lattice, Sci. China Phys. Mech. Astron. **64**, 257011 (2021).
[11] L. Xie, L. Jin, and Z. Song, Antihelical edge states in two-dimensional photonic topological metals, Sci. Bull. **68**, 255 (2023).
[12] T. Jungwirth, X. Marti, P. Wadley, and J. Wunderlich, Antiferromagnetic spintronics, Nat. Nanotechnol. **11**, 231 (2016).
[13] V. Baltz, A. Manchon, M. Tsoi, T. Moriyama, T. Ono, and Y. Tserkovnyak, Antiferromagnetic spintronics, Rev. Mod. Phys. **90**, 015005 (2018).
[14] Y.-M. Li, Y.-J. Wu, X.-W. Luo, Y. Huang, and K. Chang, Higher-order topological phases of magnons protected by magnetic crystalline symmetries, Phys. Rev. B **106**, 054403 (2022).
[15] R. Cheng, S. Okamoto, and D. Xiao, Spin Nernst Effect of Magnons in Collinear Antiferromagnets, Phys. Rev. Lett. **117**, 217202 (2016).

[16] V. A. Zyuzin and A. A. Kovalev, Magnon Spin Nernst Effect in Antiferromagnets, Phys. Rev. Lett. **117**, 217203 (2016).

[17] Z. Wang, W. Bao, Y. Cao, and P. Yan, All-magnonic Stern-Gerlach effect in antiferromagnets, Appl. Phys. Lett. **120**, 242403 (2022).

[18] T. Wimmer, A. Kamra, J. Gückelhorn, M. Opel, S. Geprägs, R. Gross, H. Huebl, and M. Althammer, Observation of Antiferromagnetic Magnon Pseudospin Dynamics and the Hanle Effect, Phys. Rev. Lett. **125**, 247204 (2020).

[19] C. Jia, M. Chen, A. F. Schäffer, and J. Berakdar, Chiral logic computing with twisted antiferromagnetic magnon modes, npj Comput. Mater. **7**, 101 (2021).

[20] M. W. Daniels, R. Cheng, W. Yu, J. Xiao, and D. Xiao, Nonabelian magnonics in antiferromagnets, Phys. Rev. B **98**, 134450 (2018).

[21] W. Yu, J. Lan, and J. Xiao, Magnetic Logic Gate Based on Polarized Spin Waves, Phys. Rev. Appl. **13**, 024055 (2020).

[22] A. Barman, G. Gubbiotti, S. Ladak, A. O. Adeyeye, M. Krawczyk, J. Gräfe, C. Adelmann, S. Cotofana, A. Naeemi, V. I. Vasyuchka, B. Hillebrands, S. A. Nikitov, H. Yu, D. Grundler, A. V. Sadovnikov, A. A. Grachev, S. E. Sheshukova, J.-Y. Duquesne, M. Marangolo, G. Csaba *et al.*, The 2021 Magnonics Roadmap, J. Phys.: Condens. Matter **33**, 413001 (2021).

[23] T. Liu, G. Vignale, and M. E. Flatté, Nonlocal Drag of Magnons in a Ferromagnetic Bilayer, Phys. Rev. Lett. **116**, 237202 (2016).

[24] Z. Hu, L. Fu, and L. Liu, Tunable Magnonic Chern Bands and Chiral Spin Currents in Magnetic Multilayers, Phys. Rev. Lett. **128**, 217201 (2022).

[25] L. Udvardi and L. Szunyogh, Chiral Asymmetry of the Spin-Wave Spectra in Ultrathin Magnetic Films, Phys. Rev. Lett. **102**, 207204 (2009).

[26] J.-H. Moon, S.-M. Seo, K.-J. Lee, K.-W. Kim, J. Ryu, H.-W. Lee, R. D. McMichael, and M. D. Stiles, Spin-wave propagation in the presence of interfacial Dzyaloshinskii-Moriya interaction, Phys. Rev. B **88**, 184404 (2013).

[27] K. Yamamoto, A.-M. Pradipto, K. Nawa, T. Akiyama, T. Ito, T. Ono, and K. Nakamura, Interfacial Dzyaloshinskii-Moriya interaction and orbital magnetic moments of metallic multilayer films, AIP Adv. **7**, 056302 (2017).

[28] Md. R. K. Akanda, I. J. Park, and R. K. Lake, Interfacial Dzyaloshinskii-Moriya interaction of antiferromagnetic materials, Phys. Rev. B **102**, 224414 (2020).

[29] M. Kostylev, Interface boundary conditions for dynamic magnetization and spin wave dynamics in a ferromagnetic layer with the interface Dzyaloshinskii-Moriya interaction, J. Appl. Phys. **115**, 233902 (2014).

[30] J. Yang, J. Li, L. Lin, and J.-J. Zhu, An origin of Dzyaloshinskii-Moriya interaction at graphene-ferromagnet interfaces due to the intralayer RKKY/BR interaction, Chin. Phys. Lett. **37**, 087501 (2020).

[31] P. Ferriani, K. von Bergmann, E. Y. Vedmedenko, S. Heinze, M. Bode, M. Heide, G. Bihlmayer, S. Blügel, and R. Wiesendanger, Atomic-Scale Spin Spiral with a Unique Rotational Sense: Mn Monolayer on W(001), Phys. Rev. Lett. **101**, 027201 (2008).

[32] Kh. Zakeri, Y. Zhang, J. Prokop, T.-H. Chuang, N. Sakr, W. X. Tang, and J. Kirschner, Asymmetric Spin-Wave Dispersion on Fe(110): Direct Evidence of the Dzyaloshinskii-Moriya Interaction, Phys. Rev. Lett. **104**, 137203 (2010).

[33] J. Cho, N.-H. Kim, S. Lee, J.-S. Kim, R. Lavrijsen, A. Solignac, Y. Yin, D.-S. Han, N. J. J. van Hoof, H. J. M. Swagten, B. Koopmans, and C.-Y. You, Thickness dependence of the interfacial Dzyaloshinskii-Moriya interaction in inversion symmetry broken systems, Nat. Commun. **6**, 7635 (2015).

[34] H. T. Nembach, J. M. Shaw, M. Weiler, E. Jué, and T. J. Silva, Linear relation between Heisenberg exchange and interfacial Dzyaloshinskii-Moriya interaction in metal films, Nat. Phys. **11**, 825 (2015).

[35] K. Di, V. Li Zhang, H. S. Lim, S. C. Ng, M. H. Kuok, J. Yu, J. Yoon, X. Qiu, and H. Yang, Direct Observation of the Dzyaloshinskii-Moriya Interaction in a Pt/Co/Ni Film, Phys. Rev. Lett. **114**, 047201 (2015).

[36] Y.-M. Li, J. Xiao, and K. Chang, Topological magnon modes in patterned ferrimagnetic insulator thin films, Nano Lett. **18**, 3032 (2018).

[37] Y. Liu, Z. Xu, Lin Liu, K. Zhang, Y. Meng, Y. Sun, P. Gao, H.-W. Zhao, Q. Niu, and J. Li, Switching magnon chirality in artificial ferrimagnet, Nat. Commun. **13**, 1264 (2022).

[38] Y. Shiota, T. Arakawa, R. Hisatomi, T. Moriyama, and T. Ono, Polarization-Selective Excitation of Antiferromagnetic Resonance in Perpendicularly Magnetized Synthetic Antiferromagnets, Phys. Rev. Appl. **18**, 014032 (2022).

[39] W. Yu, J. Lan, and J. Xiao, Polarization-selective spin wave driven domain-wall motion in antiferromagnets, Phys. Rev. B **98**, 144422 (2018).